Controlling rotational state distributions using two-pulse stimulated Raman excitation

A. S. Meijer, Y. Zhang, D. H. Parker, and W. J. van der Zande*
Institute of Molecules and Materials, Radboud University Nijmegen, Toernooiveld 1, NL-6500 GL Nijmegen, The Netherlands

A. Gijsbertsen and M. J. J. Vrakking
FOM Institute for Atomic and Molecular Physics (AMOLF), Kruislaan 407, 1098 SJ Amsterdam, The Netherlands
(Received 31 May 2007; published 17 August 2007)

The femtosecond stimulated Raman process is a versatile technique to excite rotational states in molecules. We demonstrate control over the rotational state population in a sample of NO molecules by varying the time delay between two identical laser pulses. The product of the rotational state distribution is probed by a 1+1 resonance-enhanced multiphoton ionization scheme and simulated quantum mechanically. There is good agreement between theoretical and experimental results. The product in selected quantum states shows an oscillatory dependence on the time delay. Spectral analysis reveals rotational transition energies and the presence of multiple Raman steps. We show that the relative strength of these frequency components can be related to excitation pathways with predominant $\Delta J=2$ transitions toward higher rotational states. The initial step from $J=1/2$ involves either $\Delta J=1$ or $\Delta J=2$. We find that one can discriminate between two excitation ladders. The results demonstrate the coherent effects of tailoring the shape of an ultrashort excitation pulse.

DOI: 10.1103/PhysRevA.76.023411 PACS number(s): 42.50.Hz, 32.80.Qk, 42.50.Md

I. INTRODUCTION

In studies of molecular structure and reactivity, initial quantum state preparation of the molecular sample is a vital element. Electronic, vibrational, and rotational excitation have a profound influence on bimolecular reaction rates and the outcome of photoinduced unimolecular reactions [1]. Electronic excitation alters the potential energy surfaces that are relevant to a chemical reaction, vibrational excitation alters the distribution of configurations that participate in the experiment, and rotational excitation affects the angular properties of both photonic, electronic, and atomic or molecular collisions. For instance, in atom-molecule collisions a strong influence of the collision cross sections on the alignment and orientation of the collision partners has been observed [2], while in optical experiments a strong dependence of excitation and ionization rates on molecular alignment is the rule rather than the exception [3]. Furthermore, the dependence of processes, such as high harmonic generation on molecular alignment, has recently been exploited in orbital tomography experiments where the ground state wave function of small molecules such as nitrogen has been determined [4].

In the pursuit of experimental control over molecular initial quantum state preparation, beam expansion techniques are often a first step to limit the number of states involved [5]. In a supersonic expansion substantial cooling of the internal degrees of freedom can be achieved. When combined with electrostatic multipole fields full state selection becomes possible [6]. Molecules with permanent dipole moments such as NO, OH, CH_3I, and others can be focused in specific states that may behave substantially different from the mixture of states in a beam after expansion [7]. Moreover, such selected states can subsequently be oriented so that the two "ends" of the molecule selectively point in specific directions [8].

Optical excitation provides an alternative means of preparing quantum states. Resonant photoabsorption and two-color Raman excitation or stimulated emission pumping are common techniques to state-selectively prepare atoms or molecules prior to their use in a collision experiment [9–12]. In many of these experiments the narrow bandwidth of a tunable laser or an optical parametric amplifier provides the means to control the excitation. A particularly interesting preparation scheme has been stimulated rapid adiabatic passage (STIRAP) where two narrowband nanosecond lasers are used in a counterintuitive time sequence to accomplish complete population transfer from an initial state to a selected target state [13]. STIRAP has been used to generate vibrationally pure samples [14] and can be viewed as a first example of the use of coherent control (CC) as a means to achieve quantum state preparation in a controlled manner [15–20].

More recently, efforts to control molecular quantum state preparation have increasingly made use of femtosecond laser techniques. The very short interaction time that can be achieved with femtosecond lasers means that undesirable processes such as intramolecular vibrational relaxation (IVR) can be avoided. At the same time the high peak power of most femtosecond laser sources allows for manipulation by means of nonlinear excitation.

The broad bandwidth of femtosecond pulses and the availability of tools to experimentally control the spectral amplitude, phase, and/or polarization of the pulses, provide the experimentalist with a large number of "control knobs", which allows that a quantum mechanical system can be steered into a desired quantum state. The use of these degrees of freedom under control of a genetic or evolutionary algorithm has led to the development of the popular field of laser optimal control [16,21,22].

In the present paper, we will be concerned with the application of femtosecond lasers toward controlling the prepara-

*w.vanderzande@science.ru.nl

tion of rotationally excited molecular samples as well as the molecular alignment that accompanies the excitation. When molecules are placed at the focus of an intense laser field, they undergo so-called dynamic alignment. In this process the most polarizable axis of a molecule aligns itself to the polarization axis of the laser. If the laser field is turned on and off very slowly, then the molecular axes slowly adapt to the laser field, and the alignment that occurs during the pulse disappears when the pulse is over [23]. However, if the laser pulse is turned on and off very fast, within a small fraction of the rotational period of the molecule, then the laser excitation leads to the formation of a rotational wave packet, and the molecule displays alignment both during and after the laser excitation pulse. In the latter case the alignment reoccurs under field-free conditions at revival times that are determined by the rotational constant(s) of the molecule [24,25]. Quantum mechanically, both adiabatic and nonadiabatic dynamic alignment are understood in terms of the formation of a rotational wave packet by means of a sequence of stimulated Raman transitions that couple different rotational energy levels of the ground state molecule. Dynamic alignment can be probed by means of Coulomb explosion imaging [25], by means of dissociative ionization using an ultrashort extreme-ultraviolet pulse [26] or by its manifestation in time-domain measurements [27–30]. In fact, one of the most important applications of the use of femtosecond stimulated Raman (FSR) schemes has been the development of several rotational recurrence spectroscopies, which have allowed the determination of the rotational constants of moderately large molecules [31]. Alternatively, the induced time-dependent macroscopic polarization may also be a source of ultrafast THz radiation [32], or can be used to compress the femtosecond pulses to the few-cycle limit [33,34].

Recently, Hasegawa and Ohshima [35] investigated the rotational state distribution in nonadiabatic rotational excitation of a sample of cold NO molecules by a single femtosecond pulse. They focused on the dependence of this distribution on the laser intensity and were able to identify excitation pathways typical to molecules in a doubly degenerate state. We studied the rotational excitation of NO molecules after a sequence of two identical femtosecond pulses with a variable time delay. The Fourier spectrum of the two pulses changes as function of the delay and allows one to control coherently the excitation to the different rotational levels.

Population transfer occurs whenever the energy difference between rotational states is within the bandwidth of the laser. The nonresonant transition amplitude ($\alpha^{(2)}_{FSR}$) associated with FSR processes, can—in a perturbative picture—be approximated by [36,37]

$$\Gamma^{(2)}_{FSR} \approx \int_{-\infty}^{\infty} E(\omega)E^{*}(\omega - \omega_{J,J'})d\omega, \qquad (1)$$

where $E(\omega)$ is the Fourier transform of the time-dependent electric (laser) field. J and J' provide the total angular momentum quantum numbers before and after the laser interaction, respectively. As the Stokes electric field is the complex conjugate of the pump electric field, the transition amplitude may be affected by the relative phase of the different frequencies in the pulse. In the special case of Fourier transform limited pulses, $E(t)$ is real and only the spectral amplitude of the photon pairs is relevant. By modifying the power spectrum of the ultrashort pulse, one can achieve control over the excited rotational state population. If one uses two identical femtosecond pulses with a relative time delay ΔT, then the spectral distribution contains a fringe pattern with a fringe spacing $\Delta\omega_{fr}=2\pi/\Delta T$. When a multiple of the fringe spacing matches the frequency of a rotational transition, $\Delta\omega_{fr}=n\omega_{J,J'}$, the FSR excitation probability has a maximum, since both photons necessary to drive this process are present in the spectral distribution. When the fringe period equals $\Delta\omega_{fr}=(n+\frac{1}{2})\omega_{J,J'}$, however, the transition amplitude has a minimum since at frequencies where the fringe pattern has a maximum, no suitable accompanying photons exist. We note that the FSR efficiency never becomes zero when using two pulses. From the above, we can easily predict optimum time delays for excitation to different rotational states. An alternative view of the action of the two pulses is that the first pulse produces a rotational wave packet, where the second pulse is either in phase such that the amplitude transferred by the second pulse is in phase with the amplitude transferred by the first pulse, or out of phase, such that the excited state population is coherently pumped back to the initial state.

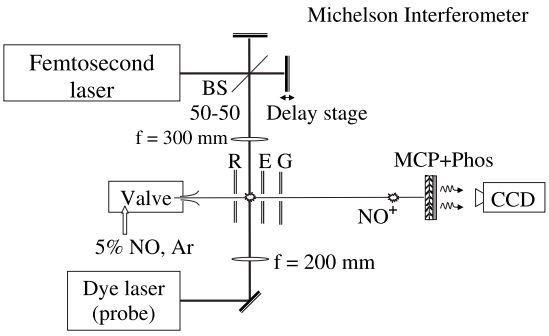

FIG. 1. A beam of rotationally cold NO seeded in Ar was expanded in vacuum and crossed by two lasers. An amplified Ti-sapphire laser is used for stimulated Raman excitation and a tunable dye laser at 20 Hz for state selective ionization of NO rotational levels. The Michelson interferometer produces two identical pulses with a relative delay between 0 and 20 ps. Ion optics transport the NO ions to a MCP detector. A CCD camera is used to quantify the NO^{+} yield.

With the intensity and bandwidth of present day femtosecond pulses, multiple Raman steps within one pulse are possible. The duration of a femtosecond pulse is considerably shorter than lifetimes and decoherence times of the created wave packets. Hence, stimulated Raman excitation is a way to coherently and selectively prepare rotationally excited samples of molecules that can subsequently be used in (collision) experiments.

II. EXPERIMENT

The experiments were performed in the setup that is depicted in Fig. 1. A molecular beam, consisting of ~2% NO seeded in Ar, was generated using a pulsed water-cooled Jor-

dan valve with a stagnation pressure of 3 bars. The valve was followed by a skimmer with an opening of 1 mm. The rotational temperature of the NO molecules was estimated to be 5 K (+5 K/−2 K), based on the measured rotational state population.

The cold NO beam was crossed by two femtosecond (pump) laser pulses with a variable time delay, up to 20 ps. The initial pulses were generated by a 1 kHz regeneratively amplified Ti-sapphire laser producing transform limited 300 μJ pulses of ~150 fs. A Michelson interferometer with a computerized motor-driven delay stage was used to split the pulse and controlled the relative time delay between the coherent pulses in time steps of approximately 0.14 ps. Temporal overlap of the pulses was deduced from the typical fringe pattern. The femtosecond pulses were focused onto the molecular beam with a 300 mm lens. The focus conditions were chosen such that no direct ionization signal was observed from the femtosecond laser. We estimate the pulse intensity at the interaction region to be equal to 2.8×10^{12} W cm^{-2}.

Population changes in each rotational state of NO where probed, 50 ns after interaction with the femtosecond pulses, using the R_{21} branch of a (1+1) resonance-enhanced multiphoton ionization (REMPI) scheme along the electronic $A\ ^2\Sigma^+ \leftarrow X\ ^2\Pi$ transition. A mildly focused 200 μJ laser pulse from a tunable dye laser, tuned around 225 nm, was used for both excitation and ionization. The frequency-doubled output of a YAG-pumped dye laser system (using Coumarin 450) had a resolution of 0.1 cm^{-1}. To enhance the signal-to-noise (S/N) ratio, the probe laser was focused with a 200 mm lens to a beam waist smaller than the pump laser.

The produced NO^+ ions were accelerated in an electrostatic field and subsequently detected by a time-gated set of microchannel plates, followed by a phosphorous screen and a charge-coupled device (CCD) camera (LaVision). The ions were defocused to avoid saturation of the multichannel plate (MCP) detector. It should be noted that the detector was built for velocity map imaging, but was not used as such in this experiment.

The 1 kHz femtosecond laser was used as master trigger and a 20 Hz signal was extracted to synchronize the YAG-dye laser system while the Jordan valve, MCP, and the camera were operated at 10 Hz. The time delay between the pump laser, the probe laser, and the molecular beam was controlled using a digital delay generator (SRS DG-535).

Multiphoton ionization of NO($A\ ^2\Sigma^+$) molecules by the femtosecond laser was used to find an overlap between the pump and probe lasers. The direct CCD signals after integration are presented in Fig. 5. The constant background in the experimental results is presumably due to $J\neq 1/2$ state population in the NO beam. The noise is attributed predominantly to power fluctuations of the dye laser as well as the femtosecond laser and intensity fluctuations of the NO molecular beam.

The experimental results will be discussed and compared to simulations in Sec. IV. Before that, we will describe the quantum mechanical treatment providing the theoretical results.

III. THEORY

The presented experiments involve multiple Raman transitions from pairs of femtosecond pulses and allow for an exact quantum mechanical treatment. The nitric oxide (NO) molecule has a degenerate $^2\Pi$ open shell ground state resulting in half integer total angular momentum quantum numbers [38–40]. The rotational energy levels of the NO molecule are given by Ref. [39], p. 103 303, providing two regular rotational ladders for the two molecular spin-orbit states

$$E_{rot}(J) = \left(J-\frac{1}{2}\right)\left(J+\frac{3}{2}\right) \pm \sqrt{4\left(J+\frac{1}{2}\right)^2 + Y(Y-4)} \mp (Y-2), \qquad (2)$$

with

$$Y = \frac{A}{B}.$$

Note that E_{rot} is dimensionless and is given in units of the rotational constant B. The spin-orbit constant A and the rotational constant necessary to calculate the rotational energy of a NO molecule in the $\nu=0$, $X\ ^2\Pi$ state are $A=123.13$ cm^{-1} and $B=1.6961$ cm^{-1} [41]. The ± sign in Eq. (2) distinguishes between (+) the upper F_2 $\left(\bar{\Omega}=\frac{3}{2}\right)$ and (−) the lower F_1 $\left(\bar{\Omega}=\frac{1}{2}\right)$ spin-orbit states ($\bar{\Omega}$ is the absolute value of the projection of the total angular momentum onto the internuclear axis Ω). For NO, the two spin orbit states differ by 121 cm^{-1} in energy. In the current work—due to cooling in the gas jet—most molecules will be in the lower (F_1) state and those in the F_2 state will be neglected.

For the $^2\Pi_{1/2}$ states that are well approximated by Hund's case (a) coupling, the Λ-type splitting is sufficiently small to be neglected in the experiments described in this work. Both Λ-doublet components (having opposite parity) are equally populated in the molecular beam. It is, however, possible (using, for example, a hexapole) to select a single component and therefore we will not sum over the Λ-doublet components $\epsilon=-1,1$ (ϵ is the symmetry index) at this point. As a consequence of the presence of the two electronic parities in NO, the selection rule of $\Delta J=2$ does not hold for Raman transitions in molecules with a Π-character ground state and $\Delta J=1$ is also allowed [42]. The total parity p of a NO rotational state is provided by Brown *et al.* [43].

$$p = (-1)^{J-\epsilon/2}. \qquad (3)$$

A Raman transition requires conservation of total parity and thus for $\Delta J=1$ it is necessary that $\epsilon=-\epsilon'$ and a $\Delta J=2$ transition can only occur if $\epsilon=\epsilon'$.

The interaction potential between a molecule and a nonresonant linearly polarized laser field can be written as [44]

$$V = -\Delta\omega\cos^2\theta + \omega_\perp = -\frac{2}{3}\Delta\omega P_2(\cos\theta) + \frac{1}{3}\Delta\omega + \omega_\perp, \qquad (4)$$

with dimensionless parameters

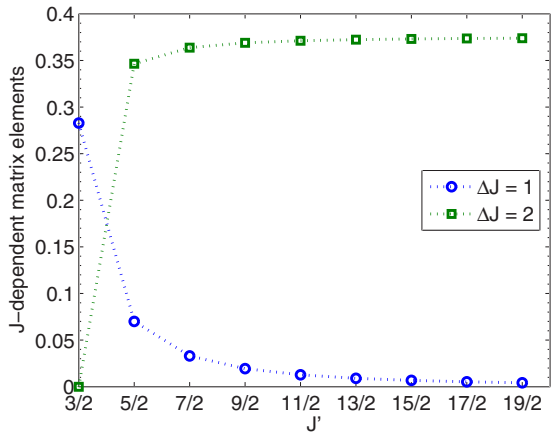

FIG. 2. (Color online) The overall J dependence of the matrix elements for $\Delta J=1$ and $\Delta J=2$ transitions. With increasing values of J, the coefficients favor a $\Delta J=2$ excitation. J' indicates the state after the laser pulse.

$$\omega_{\parallel,\perp}=\frac{\alpha_{\parallel,\perp}I_l}{2B} \quad \text{and} \quad \Delta\omega=\omega-\omega_{\perp}=\frac{\Delta\alpha I_l}{2B}.$$

In these equations, θ is the angle between the laser polarization and the molecular axis and I_l is the time-dependent laser intensity. As the term $1/3\Delta\omega+\omega_{\perp}$ is constant (independent of the rotational state) for a symmetric top, it will be neglected from here onwards. For this reason, only the polarization anisotropy $\Delta\alpha=\alpha_{\parallel}-\alpha_{\perp}$ is needed in the calculations.

The rotational part of the NO wave function [assuming Hund's case (a)] is given by

$$|J,\bar{\Omega},M,\epsilon\rangle=\frac{1}{\sqrt{2}}[|J\bar{\Omega}M\rangle+\epsilon|J-\bar{\Omega}M\rangle], \tag{5}$$

with M being the space quantization of the rotational states and total Hamiltonian by (note $M=M'$ and $\overline{\Omega}=\bar{\Omega}'$)

$$\begin{aligned}H^{M,\overline{\Omega}}_{J,J',\epsilon,\epsilon'}&=\langle J',\overline{\Omega},M,\epsilon'|H_{rot}-\frac{2}{3}\Delta\omega P_2(\cos\theta)|J,\bar{\Omega},M,\epsilon\rangle\\&=E_{rot}(J)\delta_{J',J}-\frac{1}{3}\Delta\omega\sqrt{(2J+1)(2J'+1)}\\&\times\begin{pmatrix}J' & 2 & J\\ M & 0 & -M\end{pmatrix}\left[(-1)^{M-\bar{\Omega}}\begin{pmatrix}J' & 2 & J\\ \overline{\Omega} & 0 & -\bar{\Omega}\end{pmatrix}\right.\\&\left.+(-1)^{M+\bar{\Omega}}\epsilon\epsilon'\begin{pmatrix}J' & 2 & J\\ -\overline{\Omega} & 0 & \bar{\Omega}\end{pmatrix}\right].\end{aligned} \tag{6}$$

as mentioned above, the equation predicts $\Delta J=1$ $(\epsilon'=-\epsilon)$ and $\Delta J=2$ $(\epsilon'=\epsilon)$ transitions. The J-dependent matrix elements contain the $3j$ symbols and are directly related to rotational transition probabilities. For increasing values of J, the J-dependent matrix elements clearly favor $\Delta J=2$ transitions as shown in Fig. 2. For example, for $J=1/2\rightarrow J'$, the matrix elements for $\Delta J=1$ and $\Delta J=2$ are 0.283 and 0.346, respectively, whereas for $J=5/2\rightarrow J'$, these values are 0.0329 and 0.369.

The Hamiltonian is averaged over the rapid oscillations of the laser field. For the 800 nm wavelength used and in the case of NO, the rapid oscillations can be eliminated since the laser frequency is far away from any resonances and thus the population transfer is adiabatic. Cos^2 pulses have been used in the calculations, where the laser intensity for a single pulse (within $-\tau\leq t\leq\tau$) is approximated by

$$I_l(t)=I_0\cos^2(\pi t/2\tau). \tag{7}$$

The time for the pulse to rise from zero to the peak intensity (I_0) is indicated by τ and is also the full width at half maximum of the pulse. In the time between the two laser pulses the Hamiltonian is independent of time and an analytical expression for time evolution can be used. This way, the need of numerical integration in between the two femtosecond pulses is avoided. The delay ΔT between two laser pulses is specified as the time between their maxima. The pulse sequence $I_l(t)$ is described as

$$\begin{aligned}&I_0\cos^2(\pi t/2\tau) \quad \text{for} \quad -\tau\leq t\leq\tau,\\&0 \quad \text{for} \quad \tau\leq t\leq\Delta T-\tau,\\&I_0\cos^2[\pi(t-\Delta T)/2\tau] \quad \text{for} \quad \Delta T-\tau\leq t\leq\Delta T+\tau.\end{aligned} \tag{8}$$

Note that in Eq. (8), as in Fig. 4, $t=0$ corresponds to the moment at which the first pulse reaches a maximum intensity.

With this expression for the laser intensity, we can propagate the rotational wave function by solving the time-dependent Schrödinger equation numerically as follows:

$$i\hbar\frac{\partial\Psi}{\partial t}=H(t)\Psi. \tag{9}$$

For small steps Δt,

$$\Psi(t+\Delta t)=U(t)\Psi(t), \tag{10}$$

where

$$U(t)=1-\frac{i\Delta t}{\hbar}H(t). \tag{11}$$

During both laser pulses, the wave function is propagated numerically. In between the laser pulses, the Hamiltonian is independent of time and the behavior of the wave function is described with

$$\Psi(t)=\Psi(\tau)e^{-iE_{rot}(t-\tau)/\hbar}. \tag{12}$$

The experiment involves scanning the time delay between the two identical femtosecond pulses while probing the asymptotic population of selected final states. We numerically solve Eq. (6) using $\Delta\alpha=2.8$ Å^3 [45], $\tau=150$ fs, with time steps of 0.1 fs during the laser pulses. The time delay between the pulses was varied from 0 to 20 ps in steps of 0.05 ps. The laser intensity in the experiment leads to $\Delta\omega=49$. Figure 3 shows the calculated redistribution after one pulse starting from $J=1/2$ (both Λ components equally populated). One can observe that $J=5/2$ is more populated than $J=3/2$.

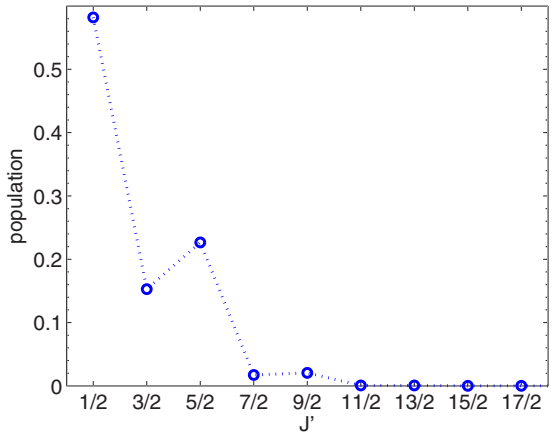

FIG. 3. (Color online) The simulated redistribution of the population to different rotational levels starting from the $J=1/2$ for a single 150 fs laser pulse ($\Delta\omega=49$). Both components of the Λ doublet are equally populated, which means that all J' states can be populated after the laser pulse. J' indicates the final state. Note, however, that the $J=5/2$ state is more populated than the $J=3/2$ state.

The redistribution of the population is highly pulse energy dependent, and toward higher intensities almost complete depletion of the ground state can be observed [35]. In Fig. 4 we present a sample calculation that follows the populations of the different states as a function of time, showing the selectivity in generating selected excited states using two 10.14 ps time delayed pulses. This sample calculation clearly shows how the use of a two pulse sequence allows selective excitation of specific rotational levels. The population of $J=3/2$ disappears by the second femtosecond pulse, whereas the populations of other states increase. Some states are pumped back by the second pulse, others grow about a factor of 4 due to the time-dependent phase of the different J states.

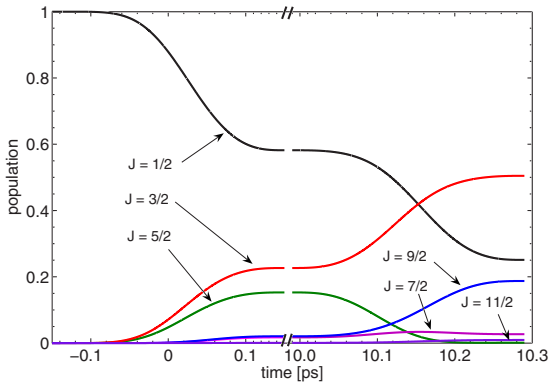

FIG. 4. (Color online) The time-dependent asymptotic population of the selected final state $J=1/2$, 3/2, 7/2, 9/2, and 11/2 using two 150 fs pulse times delayed by 10.14 ps. At this particular time delay, the second pulse favors the states $J=5/2$ and 9/2 to be populated, while $J=3/2$, 7/2, and 11/2 are almost depleted. The redistribution after the pulse sequence shows selectivity in generating selected excited states. Note that the first pulse is set to have a maximum at $t=0$.

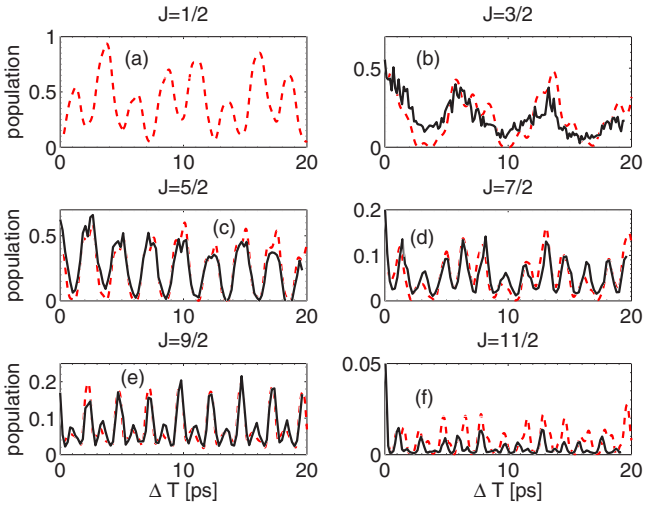

FIG. 5. (Color online) The experimental and simulated delay dependence of the NO rotational state population is depicted in six separate graphs for each final rotational state. Note that there is no experimental result for $J=1/2$. The oscillating patterns consist of multiple frequency components, revealing the presence of multiple Raman steps. The Fourier spectra of these graphs are plotted in Fig. 6.

Obviously, the two time-delayed pulses have a considerable impact on the asymptotic population transfer.

IV. RESULTS AND DISCUSSION

The dependence of the population of the NO ($J=1/2\ldots11/2$) rotational levels on the time delay between the femtosecond pulses is depicted in Fig. 5. Experimental and theoretical results are plotted in the same figure. A small and constant background signal is subtracted. This experimentally observed background is presumably due to nascent NO ($J\neq1/2$) in the beam and decreases with an increase of the final rotational state. The graphs in Fig. 6 show the Fourier spectra of the results in Fig. 5. Our calculations indicate that a depletion of the initial ($J=1/2$) state can be as large as 90% at specific time delays. An attempt to detect this depletion failed, as the high efficiency of the (1+1) REMPI process makes it impossible to limit the probe region to the focus of the femtosecond laser only. Therefore there is no experimental result for $J=1/2$ in Figs. 5 and 6. Only theoretical results are plotted in Figs. 5(a) and 6(a). Note that the sum over the rotational states of the theoretical results equals 1 for every delay.

The time traces and the Fourier spectra in Fig. 5 and Table I reveal a good overall agreement between the theoretical and experimental results for all but the highest rotational states $J=11/2$.

The simulations were preformed up to a delay of approximately 20 ps to match the experimental conditions. The peaks are labeled as $\nu_{n,m}=[E_{rot}(\frac{m}{2})-E_{rot}(\frac{n}{2})]/h$. Table I lists the relevant rotational transition frequencies as well as cross-correlation frequencies, which are the sum and difference frequencies thereof. Due to the regular spacings between the

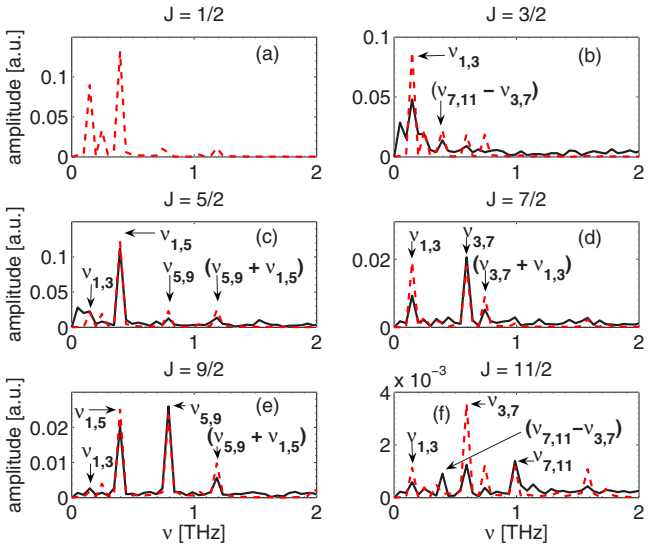

FIG. 6. (Color online) Fourier spectra of the experimental and simulated delay-dependent behavior of the population in the $J=1/2$, $J=3/2$, $5/2$, $7/2$, $9/2$, and $11/2$ rotational states. The peaks in the spectra can be assigned to rotational transition and cross-correlation frequencies as provided in Table I.

rotational energy levels, some cross-correlation frequencies in Table I are identical to transition frequencies. If the assignment could not be made unambiguously, peaks were labeled according to the highest (theoretical) transition probability as provided in Fig. 2. The height of the peaks in the Fourier spectra indicates how strong rotational transitions (and combinations thereof) are involved in populating and depopulating the concerned rotational state.

Figure 5(b) shows the result of probing the $J=3/2$ state. A dominant slow oscillation is observed corresponding to the rotational transition frequency $\nu_{1,3}$ of 0.15 THz. The smaller oscillations seen in the calculations are not resolved experimentally. That multiple frequencies play a role in populating and depopulating the $J=3/2$ level is clear from the asymmetry of the observed recurrences. These substructures are due to subsequent Raman steps to higher rotational states, which depopulate the $J=3/2$ state. The difference frequency $(\nu_{7,11}-\nu_{3,7})$ appears in the Fourier spectra, see Fig. 6(b), when a sequence of Raman steps takes place. For example, when starting from $J=3/2$, first the $J=7/2$ state may be populated, followed by excitation to $J=11/2$.

The time trace of $J=5/2$ in Fig. 5(c) shows oscillations with a period equal to a transition of $\nu_{1,5}$. Moreover, experimental dips are observed in the population near the maxima. These dips can be attributed to depletion of the rotational state $J=5/2$ due to further excitation to the $J=9/2$ state. The corresponding Fourier spectrum in Fig. 6(c) shows also a peak at 1.14 THz, which corresponds to the sum frequency $(\nu_{5,9}+\nu_{1,5})$. Note that the difference frequency $(\nu_{5,9}-\nu_{1,5})$ equals the transition frequency $\nu_{1,5}$ and cannot be distinguished. The simulations show contributions that can be labeled $\nu_{1,3}$ and $\nu_{5,9}$.

The delay-dependent population of $J=7/2$ in Fig. 5(d) shows frequencies corresponding to $\nu_{1,3}$, $(\nu_{3,7}+\nu_{1,3})$, and $\nu_{3,7}$. Note the very good agreement between experiment and simulation. Further, note that the coherence is well preserved during the 20 ps delay.

In the graph of $J=9/2$ in Fig. 6(e), two strong contributions are visible in both the experimental and theoretical Fourier spectra at frequencies $\nu_{1,5}$ and $\nu_{5,9}$. The sum frequency $(\nu_{5,9}+\nu_{1,5})$ appears in the spectra. The small contribution of the transition frequency $\nu_{1,3}$ indicates that the excitation pathway to $J=9/2$ favors two $\Delta J=2$ transitions.

At relatively high rotational levels, the delay dependence of the population becomes more complicated and more fre-

TABLE I. The oscillating population in the different rotational states has frequencies which equal rotational transition frequencies: $\nu_{n,m}=(E_{m/2}-E_{n/2})/h$ and the cross-correlation frequencies, which appear in the spectra, indicate that multiple Raman steps are made. The frequencies obtained from calculations that could not be detected in the experimental data are marked as (-).

Transition	Frequency[a] (THz)	J 3/2 [b]	J 5/2 [b]	J 7/2 [b]	J 9/2 [b]	J 11/2 [b]
$\nu_{1,3}$	0.15	0.15	0.15	0.15	0.15	0.15
$\nu_{3,5}$	0.25	-	-	-	-	-
$\nu_{5,7}$	0.35			-		-
$\nu_{1,5}$	0.40[c]		0.40[c]		0.40[c]	
$(\nu_{7,11}-\nu_{3,7})$	0.40[c]	0.40				0.40
$(\nu_{5,9}-\nu_{1,5})$	0.40[c]		0.40[c]		0.40[c]	
$\nu_{3,7}$	0.59	-		0.59		0.59
$(\nu_{3,7}+\nu_{1,3})$	0.74	-		0.74		-
$\nu_{5,9}$	0.79		0.79		0.79	
$\nu_{7,11}$	0.99					0.99
$(\nu_{5,9}+\nu_{1,5})$	1.19		1.19		1.19	
$(\nu_{7,11}+\nu_{3,7})$	1.58			-		-

[a]Calculated rotational transition frequencies using Eq. (2) [39].
[b]Experimental resolved rotational frequencies.
[c]Identical frequencies, whereas the assignment follows from Fig. 5.

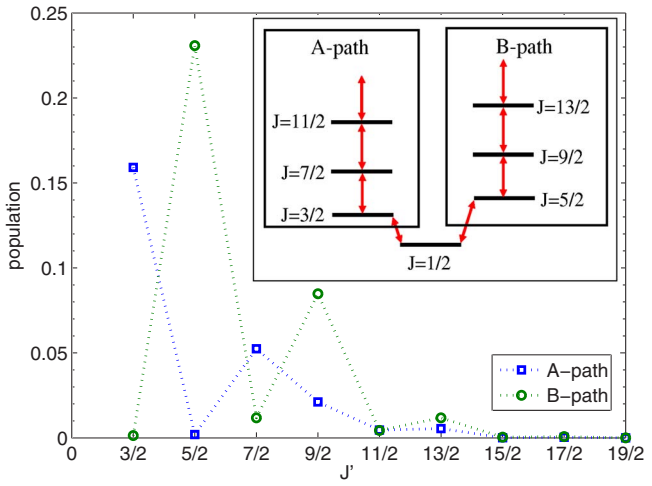

FIG. 7. (Color online) The redistributed population in the rotational states after a two pulse sequence excitation at a time delay of 6.31 ps (A path) and 10.14 ps (B path). At these particular time delays one can discriminate between two different excitation paths $A(\nu_{1,3},\nu_{3,7},\nu_{7,11},\ldots)$ and $B(\nu_{1,5},\nu_{5,9},\nu_{9,13},\ldots)$ with predominant $\Delta J=2$ transitions toward higher rotational states. The inset depicts the excitation paths from an initial state $J=1/2$.

quencies are noticeable in the spectra. The $J=11/2$ final rotational state is the highest one probed in this work. It is especially interesting as it requires at least three Raman steps starting from the ground state, encompassing a $\Delta J=1$ transition. The experimental Fourier spectrum for $J=11/2$ in Fig. 6(f) shows three transition frequencies corresponding to $\nu_{1,3}$, $\nu_{3,7}$, and $\nu_{7,11}$ with cross-correlation frequency $(\nu_{7,11}-\nu_{3,7})$.

The $J=11/2$ experimental and calculated delay-dependent populations are clearly different. This is remarkable in view of the good agreement of the other traces. The Fourier spectrum differs especially in the strength of the cross-correlation peak $(\nu_{7,11}-\nu_{3,7})$. The reason for this difference is not yet clear. Computational tests to determine whether part of the signal is due to nascent $J=3/2$ NO molecules in the molecular beam did not produce a better agreement. A possible explanation is that our Hunds case (a) approximation for the NO rotational wave function breaks down at this rotational state.

Choosing a particular time difference between the two femtosecond pulses one has control over the final rotational state distribution, but one cannot create a sample of molecules in a single excited rotational state in the current experiments. More specificity can in principle be achieved if Raman transitions are strongly saturated, which opens up the possibility of population transfer by adiabatic transfer mechanisms. In the current experiment, however, one can selectively discriminate between two different excitation paths, which we label as $A(\nu_{1,3},\nu_{3,7},\nu_{7,11},\ldots)$ and $B(\nu_{1,5},\nu_{5,9},\nu_{9,13},\ldots)$, climbing the rotational ladder with predominantly $\Delta J=2$ transitions (see the inset in Fig. 7). The first step, starting from the $J=1/2$ state, is either a $\Delta J=1$ (A-path) or a $\Delta J=2$ (B-path) transition. The formation of molecules in the $J=3/2$ state is enhanced if the delay is $\Delta T=n/\nu_{1,3}$ (with $n=1,2,\ldots$), while its formation is minimized if $\Delta T=(n-1/2)/\nu_{1,3}$. Maxima in the population of the state are found at $\Delta T=m/\nu_{1,5}$ with $m=1,2,\ldots$ while minima are observed at $\Delta T=(m-1/2)/\nu_{1,5}$. For example, the B ladder is maximized—while strongly suppressing the A ladder—at a delay of $\Delta T=10.14$ ps. By inspecting the time evolution of the different rotational states at 10.14 ps in Fig. 4 it is clearly seen that the $J=3/2$ state is depopulated by the second pulse. The same holds for a time delay between the two pulses of $\Delta T=6.3$ ps, which minimizes the population transfer via the B path.

Upon further inspection of Fig. 7 we observe nonzero populations for the $J=7/2$ in the A path and $J=9/2$ in the B path. Hence selectivity is not perfect for these states due to the presence of multiple Raman steps in each of the two fast pulses. This can be understood as the time delay is chosen to maximize selectivity at the first Raman step and in general then the following Raman steps cannot give rise to complete depopulation or maximum population. No time delay ΔT can be found such that $\Delta T=(n-1/2)/\nu_{i,i+2}$ is obeyed for multiple values of i.

V. CONCLUSIONS AND OUTLOOK

We demonstrated the ability to control the rotational state population of a sample of NO molecules by changing the time delay between two identical femtosecond laser pulses. Overall, good agreement is observed between the theoretical and experimental dependence of the population transfer on the delay between the pulses. The femtosecond stimulated Raman process is thus well understood, and this opens possibilities to create molecular samples in specific rotational state distributions. In the current experiment, however, with two delayed pulses, one cannot select any arbitrary rotational state distribution. Selectivity can be enhanced by the application of pulse shaping techniques. Even more selectivity can be realized when the Raman transitions are strongly saturated, opening the possibility for population transfer by adiabatic processes.

Our results allow us to follow the rotational excitation process. Oscillations with frequencies that correspond to transition, sum, and difference frequencies are observed in the delay-dependent population of each state. Fourier spectra of these traces reveal multiple Raman steps and the different quantum mechanical paths toward a final rotational state. The height of the peaks in the Fourier spectra indicates how strong rotational transitions are involved in populating and depopulating the concerned rotational state. A preference to climb the rotational ladder with $\Delta J=2$ transitions—a strict selection rule for most other diatomic molecules—is observed toward high rotational states. Only one strong $\Delta J=1$ transition is observed $(J=1/2\leftrightarrow J=3/2)$ and is resolved in the experimental Fourier spectra. It is this propensity for $\Delta J=2$ transitions that allows selection of the two excitation paths $A(\nu_{1,3},\nu_{3,7},\nu_{7,11},\ldots)$ and $B(\nu_{1,5},\nu_{5,9},\nu_{9,13},\ldots)$, where the initial step from $J=1/2$ is either $\Delta J=1$ or $\Delta J=2$.

Perturbation theory, which uses the photon picture, provides an intuitive insight into the coherent effects of excitation by two time-delayed broadband femtosecond pulses. The spectral amplitude of the two pulses has fringes, which can maximize or minimize the Raman transition probability.

The transition probability is maximized when the fringe spacing corresponds to a transition frequency, which equals the energy difference between the rotational levels. Both photons needed in the stimulated Raman process are then present. One (pump) photon excites the molecule to a virtual state and it is stimulated back to a rotationally excited state by the other (Stokes) photon. As long as the bandwidth of the laser pulse encompasses the rotational transition frequencies one can selectively excite and align molecules. The corresponding 2.94 THz bandwidth of a 150 fs femtosecond pulse encompasses $\Delta J=2$ rotational transition frequencies in NO up to $J=55/2$. However, the maximum rotational excitation is limited by the intensity of the femtosecond pulses [35].

We may stress that in our experiments both a time-dependent [46–50] and a time-independent molecular alignment occur. The time-independent alignment is due to the conservation of M and $\bar{\Omega}$ in the case of transitions by linearly polarized light. This alignment can be appreciated directly from our theoretical treatment and results in final states with J up to $11/2$, but always with $M=\pm 0.5$. The time-dependent alignment is due to the formation of a rotational wave packet, when using excitation pulses that are shorter than the rotational period of the molecules involved. In the present experiments we have limited ourselves to the effect of stimulated Raman transitions on the population of the rotational states, as we have no observable of the molecular alignment that is created in our molecular sample.

Future studies might involve searching for evidence of steady-state molecular alignment, as well as using pulse shaping to enhance the rotational state selectivity achieved in the current work. This technique of state selection via a femtosecond stimulated Raman process is versatile and allows one to control the rotational state distributions of dense samples of molecules. The excited and aligned molecular samples may find good use in experiments that study microscopic details of elementary processes using state selectivity and space quantization selectivity.

ACKNOWLEDGMENTS

The Netherlands Organization for Scientific Research (NWO) is gratefully acknowledged for financial support through CW and FOM. A.G. thanks Steven Stolte for useful discussions concerning the theoretical treatment described in this work. This work is part of the Stichting voor Fundamenteel Onderzoek der Materie (FOM) and was financially supported by the Nederlandse Organisatie voor Wetenschappelijk Onderzoek (NWO).

[1] R. D. Levine, *Reaction Dynamics* (Cambridge University Press, Cambridge, 2005).
[2] M. J. L. de Lange, M. Drabbels, P. T. Griffiths, J. Bulthuis, and J. G. Snijders, Chem. Phys. Lett. **313**, 491 (1999).
[3] D. Zeidler, A. Staudte, A. B. Bardon, D. M. Villeneuve, R. Dorner, and P. B. Corkum, Phys. Rev. Lett. **95**, 203003 (2005).
[4] J. Itatani, J. Levesque, D. Zeidler, H. Niikura, H. Pépin, J. C. Kieffer, P. B. Corkum, and D. M. Villeneuve, Nature **432**, 867 (2004).
[5] *Atomic and Molecular Beams Methods*, edited by G. Scoles (Oxford University Press, New York, Oxford, 1988), Vol. 14.
[6] H. G. Bennewitz, W. Paul, and C. Schlier, Z. Phys. **141**, 6 (1955).
[7] A. Gijsbertsen, H. Linnartz, G. Rus, A. E. Wiskerke, S. Stolte, D. W. Chandler, and J. Kłos, J. Chem. Phys. **123**, 224305 (2005).
[8] T. P. Rakitzis, A. J. van den Brom, and M. H. M. Janssen, Science **303**, 1852 (2004).
[9] *Molecular Dynamics and Spectroscopy by Stimulated Emission Pumping*, edited by H.-L. Dai and R. W. Field (World Scientific Publishing Co., Singapore, 1995).
[10] F. F. Crim, Annu. Rev. Phys. Chem. **44**, 397 (1993).
[11] F. F. Crim, J. Phys. Chem. **100**, 12725 (1996).
[12] A. C. Kummel, G. O. Sitz, and R. N. Zare, J. Chem. Phys. **85**, 6874 (1986).
[13] U. Gaubatz, P. Rudecki, S. Schiemann, and K. Bergmann, J. Chem. Phys. **92**, 5363 (1990).
[14] S. Schiemann, A. Kuhn, S. Steuerwald, and K. Bergmann, Phys. Rev. Lett. **71**, 3637 (1993).
[15] P. Brumer and M. Shapiro, *Principles of the Quantum Control of Molecular Processes* (Wiley, New York, 2003).
[16] W. S. Warren, H. Rabitz, and M. Dahleh, Science **259**, 1581 (1993).
[17] B. Broers, L. D. Noordam, and H. B. van Linden van den Heuvell, Phys. Rev. A **46**, 2749 (1992).
[18] D. Meshulach and Y. Silberberg, Phys. Rev. A **60**, 1287 (1999).
[19] J. K. Ranka, R. W. Schirmer, and A. L. Gaeta, Phys. Rev. A **57**, R36 (1998).
[20] N. Dudovich, D. Oron, and Y. Silberberg, Phys. Rev. Lett. **88**, 123004 (2002).
[21] R. S. Judson and H. Rabitz, Phys. Rev. Lett. **68**, 1500 (1992).
[22] J. L. Herek, W. Wohlleben, R. J. Cogdell, D. Zeidler, and M. Motzkus, Nature **417**, 533 (2002).
[23] H. Stapelfeldt and T. Seideman, Rev. Mod. Phys. **75**, 543 (2003).
[24] M. J. Vrakking and S. Stolte, Chem. Phys. Lett. **271**, 209 (1997).
[25] F. Rosca-Pruna and M. J. J. Vrakking, Phys. Rev. Lett. **87**, 153902 (2001).
[26] F. Lepine, Kling, Y. Ni, J. Khan, O. Ghafur, T. Martchenko, E. Gustafsson, P. Johnsson, K. Varju, and T. Remetter *et al.*, J. Mod. Opt. **54**, 953 (2007).
[27] J. P. Heritage, T. K. Gustafson, and C. H. Lin, Phys. Rev. Lett. **34**, 1299 (1975).
[28] C. H. Lin, J. P. Heritage, T. K. Gustafson, R. Chiao, and J. McTague, Phys. Rev. A **13**, 813 (1976).
[29] M. Morgen, W. Price, L. Hunziker, P. Ludowsie, M. Blackwell, and Y. Chen, Chem. Phys. Lett. **209**, 1 (1993).
[30] T. Seideman, Phys. Rev. Lett. **83**, 4971 (1999).
[31] P. M. Felker and A. H. Zewail, Adv. Chem. Phys. **70**, 265

(1988).
[32] N. G. Kalugin and Y. V. Rostovtsev, Opt. Lett. **31**, 969 (2006).
[33] A. Nazarkin and G. Korn, Phys. Rev. A **58**, R61 (1998).
[34] N. L. Wagner, E. A. Gibson, T. Popmintchev, I. P. Christov, M. M. Murnane, and H. C. Kapteyn, Phys. Rev. Lett. **93**, 173902 (2004).
[35] H. Hasegawa and Y. Ohshima, Phys. Rev. A **74**, 061401(R) (2006).
[36] N. Dudovich, B. Dayan, S. M. Gallagher Faeder, and Y. Silberberg, Phys. Rev. Lett. **86**, 47 (2001).
[37] D. Oron, N. Dudovich, D. Yelin, and Y. Silberberg, Phys. Rev. Lett. **88**, 063004 (2002).
[38] G. Herzberg, *Molecular Spectra and Molecular Structure, Spectra of Diatomic Molecules* (Van Nostrand and Reinhold Company, New York, 1960)**,** Vol. 1.
[39] R. N. Zare, *Angular Momentum: Understanding Spatial Aspects in Chemisty* (John Wiley and Sons, New York, 1988).
[40] J. M. Holas, *Angular Momentum: Understanding Spatial Aspects in Chemisty and Physics Spectroscopy*, 3rd ed. (Krieger Publishing Co., Modern Malabar, 1996).
[41] C. Amiot, J. Mol. Spectrosc. **94**, 150 (1982).
[42] F. Rasetti, Phys. Rev. **34**, 367 (1929).
[43] J. M. Brown, J. T. Hougen, K. P. Huber, I. K. J. W. C. Johns, H. Lefebvre-Brion, A. J. Merer, D. A. Ramsay, J. Rostas, and R. N. Zare, J. Mol. Spectrosc. **55**, 500 (1975).
[44] B. Friedrich and D. Herschbach, J. Phys. Chem. **99**, 15686 (1995).
[45] B. Friedrich and D. Herschbach, J. Phys. Chem. A **103**, 10280 (1999).
[46] H. Stapelfeldt and T. Seideman, Rev. Mod. Phys. **75**, 543 (2003).
[47] T. Seideman, J. Chem. Phys. **103**, 7887 (1995).
[48] M. J. J. Vrakking, D. M. Villeneuve, and A. Stolow, Phys. Rev. A **54**, R37 (1996).
[49] F. Rosca-Pruna, E. Springate, H. L. Offerhaus, M. Krishnamurthy, N. Farid, C. Nicole, and M. J. J. Vrakking, J. Phys. B **34**, 4919 (2001).
[50] E. Springate, F. Rosca-Pruna, H. L. Offerhaus, M. Krishnamurthy, and M. J. J. Vrakking, J. Phys. B **34**, 4939 (2001).